Optical Engineering

RESEARCH PAPER

Digital glass forming of photonics

Nicholas Capps,[a] Chen Zhu,[a] Jonathan Goldstein,[b] and Edward Kinzel[a],*
[a]University of Notre Dame, Aerospace and Mechanical Engineering, Notre Dame, Indiana, United States
[b]Air Force Research Laboratory, Wright-Patterson AFB, Ohio, United States

ABSTRACT. We investigate the digital glass forming process for depositing commercial SMF-28 single-mode optical fiber for photonic purposes. The process utilizes a CO_2 laser to locally heat the feedstock to fuse it onto a fused quartz substrate. We focus on how altering the deposition parameters, including the laser power, feed rate, and path plan, affects the deposited fiber morphology and how this affects the optical transmission. At high powers, the fiber bonds strongly to the substrate, resulting in significant changes in fiber morphology and core shape. With a gradient transition between the feedstock geometry and the deposition geometry, high optical transmission for straight line depositions can be achieved. Additional work was performed examining the optical losses when the fiber is deposited around a constant radius curve for different fiber morphologies, with higher losses recorded for higher power samples. Comparing the doping profile of these samples indicates that the gradient of Ge decreases at higher laser power, suggesting the losses are caused by diffusion of the fiber core. This work shows that for high input powers, the optical losses around curves are increased, leading to a tradeoff between the bonding strength and optical transmission for these geometries.

[DOI: 10.1117/1.OE.62.7.076101]

Keywords: additive manufacturing; glass; photonics

Paper 20221498G received Dec. 29, 2022; revised Jun. 26, 2023; accepted Jul. 5, 2023; published Jul. 25, 2023.

1 Introduction

1.1 Background

Silicate based glasses are used for a wide variety of optical applications. They are attractive materials for a number of structural and scientific components (e.g., wafer boats and chemistry glassware). This utility is due to the material's transparency from the near ultraviolet (UV) to near infrared (IR) wavelengths, high thermal stability at elevated temperatures, stiffness, scratch resistance, formability at high temperatures, and the ability to dope the material to change its optical and chemical properties.[1–3]

There has been considerable interest in utilizing additive manufacturing (AM) techniques to create optical and photonic devices from silica-based glasses. However, the high molten viscosity and high transparency of glass in the near-UV to NIR wavelength range pose a challenge to the most common AM methods. There are significant difficulties with bubble evacuation within powder-based approaches, leading to mechanically weak and low transmission parts.[4] There have been some successful methods for creating transparent glass AM structures such as a composite method using nanophase silica precursor-loaded polymer slurries. These are deposited into green bodies using conventional AM processes, such as direct ink writing or stereolithography. These parts are then dried, pyrolyzed, and densified following ceramic processing techniques to produce dense 3D glass structures. However, there are challenges to utilizing this method for

---

*Address all correspondence to Edward Kinzel, ekinzel@nd.edu creating parts with high aspect ratios due to limited build volume and part shrinkage, and the method also suffers from low cycle time.[5–7] Other methods use a traditional fused filament fabrication approach to deposit glasses but utilize specialized tooling or alternative feedstock chemical compositions (e.g., chalcogenide) to overcome the high temperature requirements for glass deposition.[8,9]

Another glass AM methodology utilizes a CO_2 laser to locally heat solid silica glass feedstocks to deposit the material directly onto a substrate of the same material.[10–12] While these AM systems have been used to produce small parts via layer-by-layer deposition, relatively little work has been done to explore the utilization of the material's optical properties for waveguiding and photonic devices.[4,8–11] This is despite the already robust infrastructure for the high-volume production of optical fiber feedstocks and the customizability of the feedstock geometry and chemistry. While there have been successful depositions of coreless silica fibers, the absence of a core limits the optical transmission.[12] This presents a knowledge gap in the glass AM community to deposit high transmission optical fiber parts for several application spaces. These are primarily focused on sensing applications, such as depositing optical fiber onto lenses and optical components for temperature monitoring, as well as photonic sensors integrated into larger systems. This motivated the work in this paper, which focuses on the challenges and viable process parameters for depositing high-transmission single-mode optical fiber utilizing the digital glass forming (DGF) deposition approach. This is done by establishing empirically defined relationships between the input parameters such as feed rate and input laser power, and the fiber's deposition behavior, including the resulting fiber morphological parameters. The goal of this research is to develop process parameters that deposit fibers that are robustly bonded to the substrate while preserving high optical transmission in both straight sections and around curves.

1.2 Experimental Setup

Figure 1 depicts the DGF technique applied to printing optical fiber. In this setup, the stripped optical fiber feedstock (Corning SMF-28) with an outer diameter of 125 μm (denoted as A in the figure) is fed into the intersection between a CO_2 laser beam (Iradion 1625, $\lambda_0 = 10.6\ \mu\text{m}$) and a fused quartz substrate (B). This wavelength of radiation couples very strongly to the vibrational modes of the SiO_2 matrix (phonons), making silicate-glasses highly absorptive at 10.6 μm. Due to this high absorptivity, the laser is approximated as a surface heat flux applied to both the feedstock and illuminated area on the substrate.[13] The substrate is mounted to a four-axis positioning system using computer-controlled stages (Aerotech ANT130XY, ATZ100 and ANT130R). By feeding in the fiber while the workpiece is translated, 2D structures can be created on the substrate.

For building effective, robust photonic devices, the deposited fiber structure must both be optically transmissive and strongly bonded to the supporting substrate. To achieve strong fusion between the feedstock and the substrate, the bottom surface temperature of the fiber must be high enough so the two materials can coalesce and flow together. The high temperature gradients produced by this process can lead to the development of thermal stresses inside the material, but due to fused silica's low coefficient of thermal expansion, these stresses are lower than the fracture strength of the material.[14] This allows for the material to be deposited "cold" (at room temperature) with no preheat or post-process annealing required, although there are residual thermal stresses retained in the part.

As received, the fiber is protected in an acrylate coating, which is removed before deposition, as unreported previous experiments have shown a black carbon residue left on the fiber surface after deposition. This residue, along with dust and oil residue from contact with the skin can cause significant defects in the fiber deposition. As such, the acrylate is removed by first soaking a length of fiber in commercial grade acetone for >30 mins. From there, the fiber is mechanically stripped as needed, and excess feedstock may be placed back in acetone to protect against dust and other contaminants. The stripped fiber is handled with nitrile gloves to prevent contamination. These experiments were performed in a non-clean room environment, so to further protect the produced part, the feedstock fiber is wiped with isopropyl alcohol (IPA)-soaked lens paper immediately before deposition.

As shown in Fig. 1, the fiber is directed into the substrate through the steel guide tube (C), bending gently until the fiber surface is tangent to the substrate. To maintain high optical

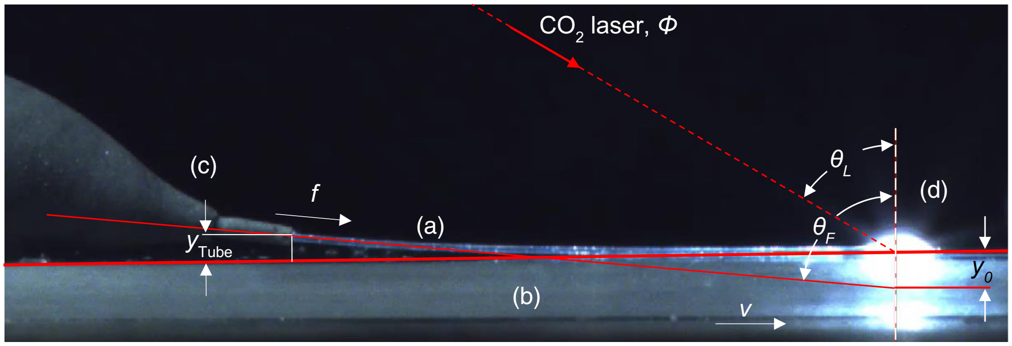

Fig. 1 Diagram of the DGF deposition annotated with input parameters. This shows the optical fiber (a) directed toward the fused quartz substrate (b) through the feed tube (c). The laser intersects with the fiber/substrate at (d).

transmission through the fiber, the deposited material must remain free of small bends or deflections in the fiber. From anecdotal results, these macro-bend defects most easily appear at the start and end of the deposition, particularly if the fiber is not tangent with the substrate where the laser intersects it. Conceptually, the feeder angle θ_F could be set to a wide range of angles so long that it is larger than the incident laser angle θ_L and the resulting fiber is tangent to the substrate. However, it was found through qualitative experiments that keeping a very shallow approach ($\theta_F = 81\ \mathrm{deg}$) gave the best experimental results. To deliver the optical fiber to the substrate, the feedstock is guided through a feed tube made from concentric hypodermic tubes, the smallest of which has a manufactured internal diameter between $160 \pm 20\ \mu\mathrm{m}$. This tube diameter allows up to $55\ \mu\mathrm{m}$ of fiber displacement inside the feed tube. These displacements can cause light scattering micro-bends to appear in the fiber during deposition, but these can be reduced by depositing the fiber as close to the center of the laser spot as possible. For the alignment process, two high resolution video cameras were used, oriented to view the process from the side and from the top. The filament feeder is attached to three-axis manual micrometer stages for precise positioning of the fiber into the center of the laser spot. For the experiments reported in this paper, the center of the feed tube is positioned at $y_\mathrm{Tube} = 125 \pm 25\ \mu\mathrm{m}$ from the top surface of the substrate, and the center of the laser spot was selected to intersect with the substrate 3 ± 0.05 mm away from the feed tube. The geometric parameters define that the intersection between the nominal fiber feed vector and the center of the laser spot on the substrate is at $y_0 = 300 \pm 25\ \mu\mathrm{m}$, which defines the curve of the fiber. The $\mathrm{CO_2}$ laser beam of average power Φ and normal spot size diameter of 2.65 mm ($1/\mathrm{e}^2$) is incident on the substrate at $\theta_\mathrm{L} = 60\ \mathrm{deg}$, and the fiber is centered in the plane defined by this laser and the substrate normal.

2 Deposition Morphology

2.1 Diameter Control and Fiber Morphology

By underfeeding or overfeeding the fiber feed rate f relative to the table scan speed v, the melt pool can be viscously deformed to control the resulting cross-sectional area. To identify some of the important characteristics of this effect, a process parameter sweep was performed to examine the relationship between the feed rate parameters and the resulting fiber morphology. For this experiment, f was kept constant at $6.75\ \mathrm{mm/s}$, whereas v was varied to achieve a desired f/v ratio was swept in $f/v = 0.1$ increments until the deposition failed. The laser power $\Phi = 57.5\ \mathrm{W}$ was empirically determined for $f/v = 1$ to deposit a continuous track that is well bonded to the substrate. The failure points were identified by a breakdown in the normal deposition behavior. For instance, sufficiently underfed fiber ($f/v = 0.4$) begins to oscillate in diameter from 80 to 90 μm with an average spatial period of 765 μm. This behavior is consistent with Rayleigh instabilities as the molten fiber diameter decreases to a minimum.[15] After deposition, the fibers were encased in a black epoxy before they were cross sectioned in 10-mm-thick sections and polished. After, the section was viewed under the microscope using a 20× objective while back-illuminated using an unpolarized light source, as shown in Fig. 2 below. The resulting fiber cross sections are shown below in Fig. 3, which clearly shows the source light coupling to

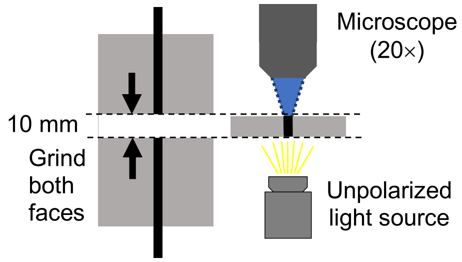

Fig. 2 Diagram of microscopy of deposited samples.

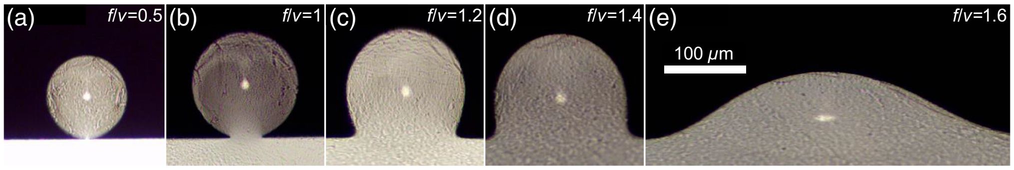

Fig. 3 Micrographs of fibers produced at $\Phi = 57.5$ W and $f = 6.75$ mm/s with increasing f/v from (a) to (e). Note the bright fiber core contrasting with the darker cladding.

the fiber core visible by the brighter area in the center of the fiber. The cross-sectional area of the fiber of each deposition was captured in ImageJ after trimming the substrate and surrounding black epoxy from the image. As such, the error in the cross-sectional area is expected to be on the order of the pixel resolution for the image (<1 μm). Unless otherwise stated, all images in a figure use the same scale bar.

The fiber cross-sectional area was extracted for each sample, which was then compared against the expected area assuming conservation of volume. This is shown in Fig. 4 below, which highlights two deposition regimes for $f/v \leq 1$ (A - B) and $f/v > 1$ (C - E), respectively. For ratios less than 1, the cross-sectional area remains consistent with the expected area until the data point at $f/v = 0.4$, where there is a sharp deviation from the expected value. This deviation is caused by the oscillating fiber diameter, where the sample happened to be sectioned in one of the thicker sections of the deposition. As shown, decreasing the f/v ratio decreases the deposited volume while maintaining the circular shape of both the fiber cladding and the core. It is worth noting that as the f/v ratio decreases, the deposited fiber bonds only very weakly to the substrate and can be easily removed using a fingernail. This is caused by the decrease in laser exposure time caused by the faster scan speed v. This suggests that this oscillation behavior might be mitigated by a change in Φ or baseline f to give a more advantageous heating profile on the glass surface.

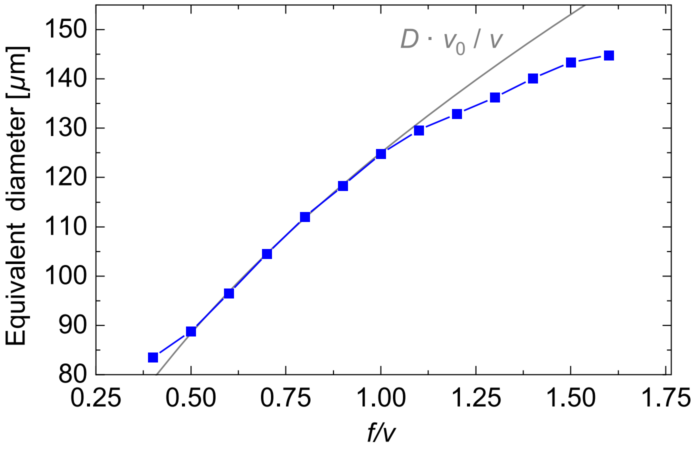

Fig. 4 Resulting fiber area normalized to the expected fiber area assuming conservation of volume.

Inversely, for $f/v > 1$, the fiber can be clearly observed deforming from the nominally circular geometry and flow into the substrate, resulting in a highly distorted fiber shape. Fibers with this general morphology are termed as "slumped" to the substrate and have a significantly stronger bond strength. As shown in Fig. 4, at higher ratios the resulting area is significantly smaller than the values calculated from conservation of volume. This behavior may be explained by fiber vaporization caused by a longer exposure time (lower v). The maximum overfeed ratio recorded for this power was $f/v = 1.6$, where the fiber buckles to the side out of the laser spot. One possible explanation for this is that so much glass is fed into the laser spot that the bottom of the fiber remains cool during deposition, increasing the viscosity and causing the feedstock to buckle under the increased resistive forces. The visible core cladding structure suggests the deposited fibers should still be capable of guiding light for both adhered and slumped fibers.

2.2 Dependence of Transmission on Coupling Length

For a defined set of v, Φ was swept to empirically define the relationships between laser power, the resulting fiber morphology, and optical transmission. For this experiment, the fiber was deposited on the substrate for 75 mm at a constant $f/v = 0.985$. This ratio was selected to maintain a small, uniform tension on the fiber during deposition, avoiding any buckling behavior that may develop when the fiber is under a compressive load. Examples of the resulting morphologies for $v = 6.75$ mm/s are shown below in Figs. 5(a)–5(f). As shown in the lowest power samples, the core of the optical fiber appears to remain undisturbed by the deposition, however it is clearly seen that the contact area between the optical fiber and substrate is extremely small, only ∼20 to 50 μm in length, resulting in a mechanically weak bond. A stronger bond can be achieved with higher laser power, but the micrographs of these samples show a significantly distorted elliptical core shape. However, the contrast between the core and cladding remains, suggesting some light guiding capabilities remain. The core shape of these samples is similar to elliptical core geometries used for polarization maintaining fibers.[16]

To measure the transmission through the fiber, an optical fiber fusion splicer (Fujikura FSM-50S) was used to connect the produced samples between a broadband non-polarized light source, (YSL Photonics SC-5-FC) and an optical spectrum analyzer (OSA) (Ando AQ6317B). By comparing the transmitted optical signal of the deposited fiber against a known reference (unprocessed optical fiber of the same length), the relative transmission can be measured. For this paper, the transmission was integrated over the optical C-band (1530 to 1565 nm), which is a common testing bandwidth for SMF-28 fiber. The integrated fiber signal is normalized against the transmission through a reference SMF-28 fiber of the same length as the sample. This normalized transmission spectrum is shown below in Fig. 6 for experimental depositions at different powers. For the deposited samples to be fusion spliced between the light source and OSA, the deposition must extend ∼60 to 80 mm out from the edge of the substrate to fit within the dimensions of the splicer. To achieve these unsupported fiber lengths, the one of these fiber leads must be fed out before the start of the deposition, and several centimeters of unheated fiber is deposited over the edge of the substrate at the end of the deposition to decouple the two materials. Additionally, since the unsupported fiber leads are unheated, for a high-power deposition,

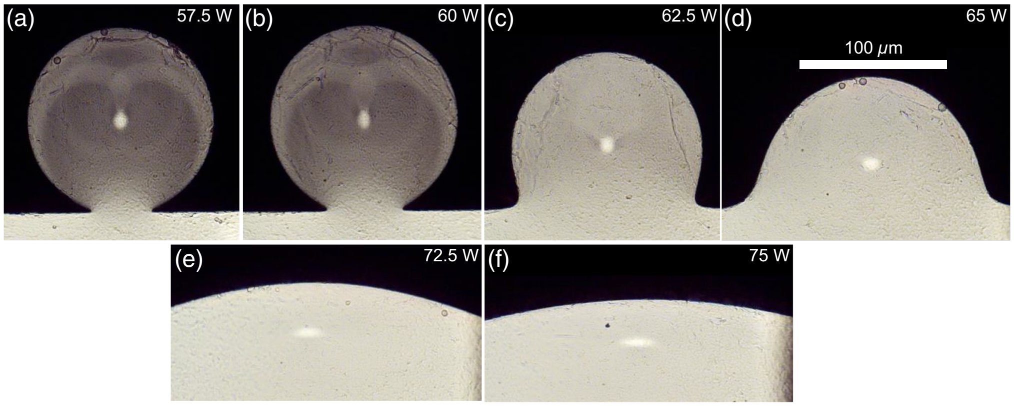

Fig. 5 (a)–(f) Fiber cross-section as a function of increasing laser power at $v = 6.75$ mm/s.

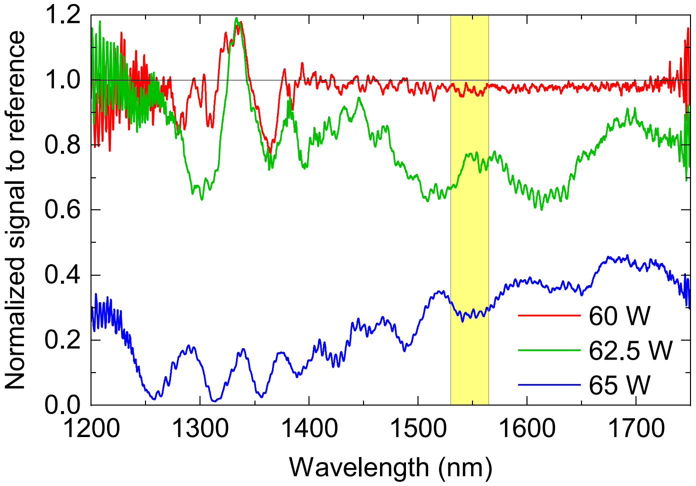

Fig. 6 Transmitted power spectrum of some example fibers deposited at various powers.

there is a significant morphology change between the slumped fiber and the unprocessed circular fiber, causing the high transmission losses seen in Fig. 6.

Since the morphology is determined by the heating profile, the laser power was set to linearly increase and decrease over some transition length at the ends of the deposition. As shown in Fig. 5, the morphology for $v = 6.75\ \mathrm{mm/s}$ is only sensitive to the laser power above 55 W. As such, the transition length L_c was defined to be the distance where Φ would increase from 55 W to the final processing power of the deposition. This minimum starting Φ was empirically determined for other deposition rates using the same process.

For this experiment, Φ was swept in 2.5 W increments from this minimum laser power through the point where a significant amount of vaporization occurred, removing much of the cladding around the fiber core. Additional samples were filled in at 1 W increments, where necessary to capture the trends. This experiment was repeated for several L_c, to observe its effect on the optical transmission. The results of this experiment are highlighted in Fig. 7(a) below. As shown for both data sets, at low Φ, the optical fibers retain high transmission ($\tau = \sim 0.95$). However, for the short transition length samples ($L_c = 3.75$ mm), there is a critical cutoff power around 62.5 W where the fiber transmission drops off. From Fig. 5, this power is where the fiber morphology begins to significantly change. For the longer L_c specimens, optical transmission is retained even at the highest laser powers. To further highlight the effect that L_c has on τ, the experiment was repeated at $\Phi = 70$ W for several L_c values. The results of this experiment are shown in Fig. 7(b), which highlights the high sensitivity of the transmission against the power transition length. As shown, the optical transmission at 15 mm transition length begins to approach the maximum transmission of the measured samples, so this length was used for all subsequent experiments in this paper. The error bars in the optical transmission are defined by the variation in transmission caused by the fusion splicer. This was captured by measuring the

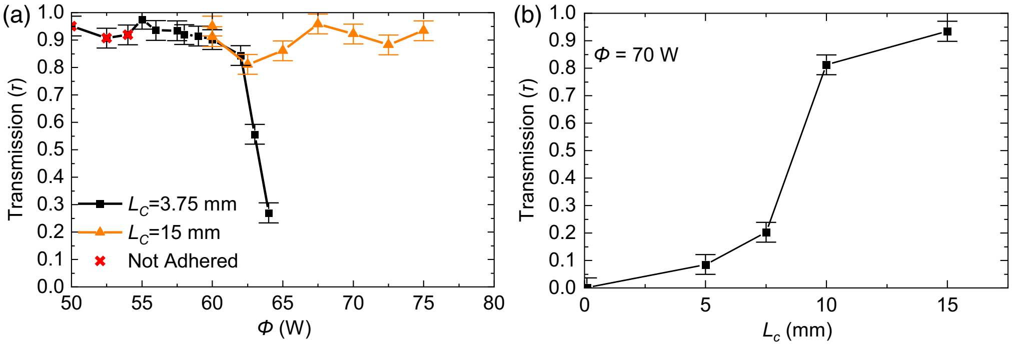

Fig. 7 Comparison of the transmission as a function of (a) Φ and (b) L_c.

transmission across ten samples of unprocessed fiber (150 mm long) spliced between the light source and OSA.

2.3 Dependence of Curved Transmission on Morphology

To act as an effective waveguide, deposited fibers must not only have strong adhesion to the substrate and high transmission but also must retain this high transmission around curves and corners. For pristine fiber, the losses around bends (>1 mm radius) are modeled by the Beer Lambert law. The expected transmission around a curved section is expected to follow an exponential decay by $\tau = \exp(-\alpha L)$ where τ is the optical transmission, α is a scattering value that is related to the radius of curvature R and arc angle θ, and L is the length of the curve such that $L = R\theta$.[17,18] The scattering value is dependent on the fiber design and wavelength, where longer wavelengths are more sensitive to bending radius than shorter wavelengths. However, depositing the fiber using the DGF method may cause significant changes to the scattering value, which required additional experimentation and study.

Fiber arcs of some defined radius R and angle θ were deposited on the substrate. The curve was designed to have straight leads longer than length L_c the ends of the arc, to allow for the required power transition length. The path plan was designed to incorporate both linear and rotation stages to maintain a constant linear velocity tangent to the desired curve. By incorporating both stages, arbitrary curved geometries can be created so long as the substrate is large enough to accommodate it.[19] The experiment was designed to examine the relationship between arc geometry and fiber morphology to the resulting optical transmission. The tacked (weakly fused) fibers were produced at $\Phi = 57.5$ W with $v = 6.75$ mm/s, whereas slumped fibers were created at $\Phi = 33$ W with $v = 1$ mm/s. The transmission as a function of arc length for the tacked samples are shown below in Fig. 8, which fits well to the Beer-Lambert law. Additionally shown in Fig. 8 is a photograph of the light leaking out of a 5 mm radius sample.

There has been considerable effort applied to modeling the bending attenuation for a cylindrical step-index fiber design, based on an analysis of the electric field propagation using the physical parameters of the fiber.[17,18,20] However, these equations are cumbersome to apply for an arbitrary fiber geometry and assume a circular step index core, which may not be the case for the slumped fiber geometry. One successful method semi-empirically simplified the bending losses as a function of radius, as reported by Tsao and Cheng.[20] Their approach models the losses an exponential $L_R = \eta_1 \exp(-\eta_2 \cdot R)$, where η_1 and η_2 are wavelength-dependent fitting parameters.[20] Normalizing the losses around a curve by the length of the arc allows for direct comparison of fibers with different morphologies on a single graph. As shown in Fig. 9, the transmission losses for the high-power slumped fiber are significantly higher than the other datasets. This data show that depositing the fiber on the substrate induces additional losses and those losses are expected to become more substantial with higher powers. This effect can be seen in Fig. 10, where the same deposition profile ($R = 15$ mm, $\theta = 30$ deg, $v = 1$ mm/s) was deposited at varying laser powers, showing significantly higher losses as the deposition power increases.

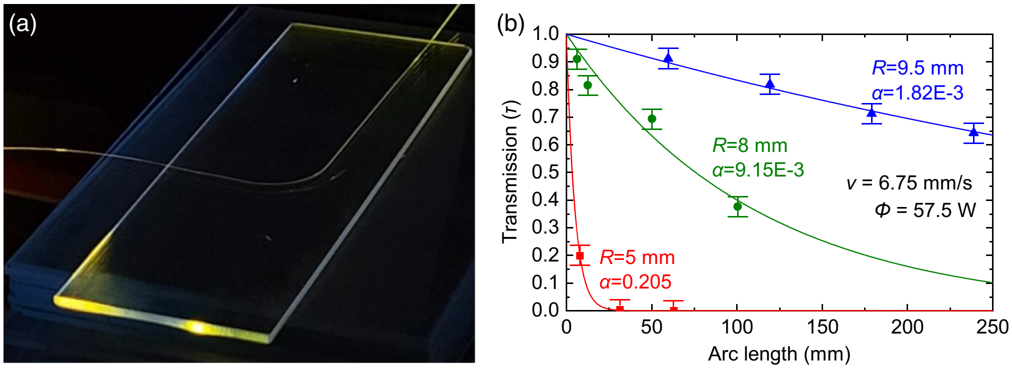

Fig. 8 Transmission as a function of arc-length.

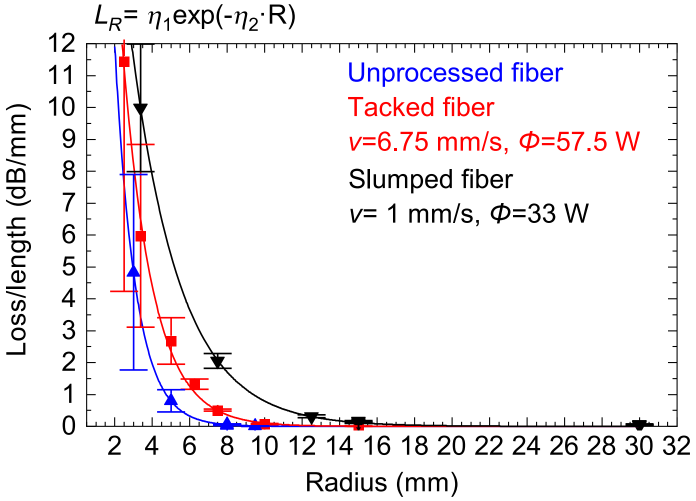

Fig. 9 Losses/length for number of radii and fiber cross-section profiles.

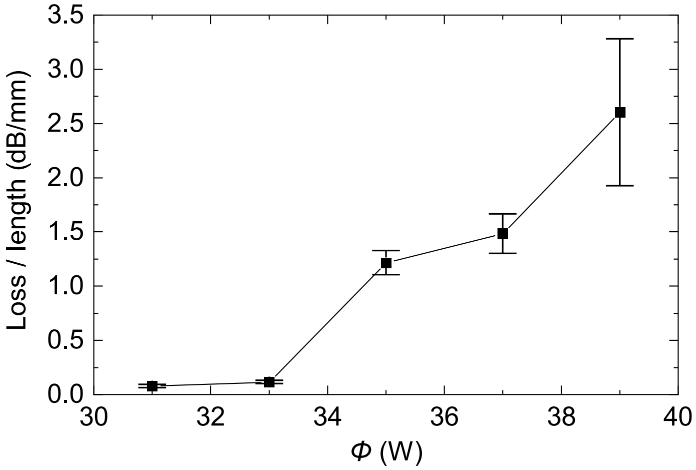

Fig. 10 Transmission around a 15 mm, 30 deg arc curve at 1 mm/s as a function of Φ.

3 Discussion

3.1 Core Geometry

As seen in the cross sections shown in previous figures, producing slumped fiber significantly distorts and elongates the nominally 8 μm Ge doped core of the fiber. From literature, it is known that the change in index of refraction is related to the Ge content within the Si-O glass matrix, so a change in the Ge contrast may allow for increased light leakage.[21,22] Using energy dispersive X-ray analysis (EDX), a spatially resolved chemical composition of the fiber cross-section can be extracted, allowing for a faux-colored overlay representing the Ge content of the fiber to be overlayed with scanning electron microscope (SEM) images. Example images for tacked and slumped fiber morphologies with colored Ge content overlayed are shown below in Fig. 11. Additionally shown is a zoomed in color map of the corresponding core for each fiber. Additionally, the weight percentage profiles for the three fibers can be extracted for comparison by single line scans across the center of the core. Since the core of the slumped fiber is elliptical in shape, two scans were performed along its major and minor axes.

The resulting scans are shown below in Fig. 12. As shown, the extracted profile for the unprocessed fiber approximates a step index with a uniform Ge profile across the core, and this profile shape remains unchanged for the tacked profile. For the slumped fiber, the Ge profile is significantly smoothed, resulting in a much wider core with a smaller Ge gradient between the

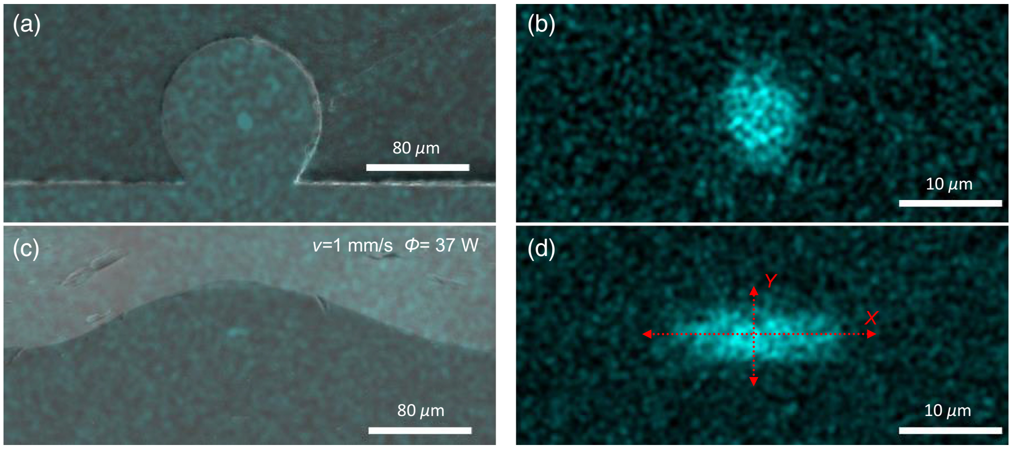

Fig. 11 Faux-colored SEM of the tacked fiber (a), with zoomed EDX image highlighting the fiber core (b). Slumped profiles in panels (c) and (d).

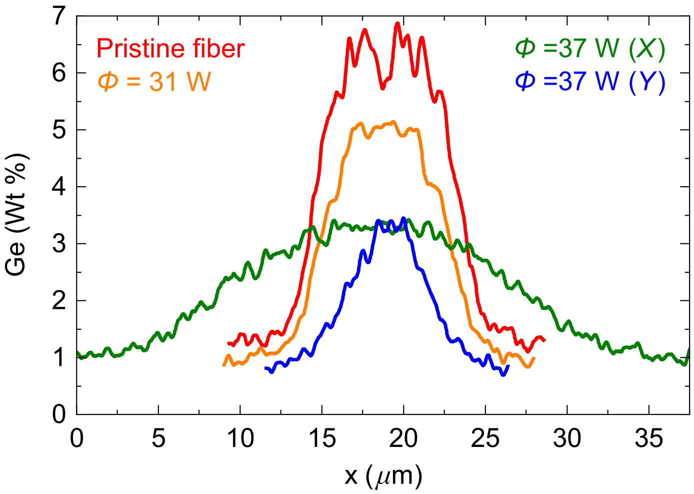

Fig. 12 EDX extracted Ge profile for the fiber cores.

core and cladding. Additionally, the peak Ge content of the core is no longer uniform over the cross-section, instead appearing Gaussian in shape. Fitting a Gaussian curve to this experimental data, the full-width half maximum (FWHM) of the core diameter for the feedstock and tacked fibers are calculated to be 8.5 μm and 7.6 μm, respectively. The slumped fiber core had grown significantly wider, to dimensions of 18.9 $\mu\text{m} \times 5.3$ μm for the major and minor axes, respectively. Calculating the cross-sectional area for these dimensions, the area of the slumped fiber core is ∼1.4 times larger than the unprocessed fiber, with a weaker Ge gradient and lower overall Ge content. These changes suggest that diffusion of Ge from the core into the cladding increases the light leakage when going around corners. Additionally, the stress profile that is produced when depositing fiber can affect the fiber's index profile (from birefringence), which may explain the increased light losses for tacked fiber. However, both effects may be able to be compensated for by variations in design, as larger radius curves have increased transmission, approaching the saturation transmission of straight-line fiber.

3.2 3D Paths

Future work on this process is being focused on two design applications. This paper has shown that fibers deposited using the DGF method can maintain optical transmission around curves of a sufficient diameter. However, to create photonic circuits, two deposited fibers must be coupled together such that evanescent waves from one fiber core can be coupled into another. In literature,

Fig. 13 Printing a small spiral structure built using DFG and a 125 μm diameter optical fiber.

single mode fibers must undergo special processing to be coupled together, such as shaving the cladding on one side to place the cores closer to each other.[23] However, because of the fine diameter control available by altering f/v, it may be possible to deposit elongated microfibers such that the two cores can couple together. Additionally, by depositing two slumped fibers on top of each other, the cores of the fibers may approach each other because of gravity. Alternatively, larger core multi-mode fibers are available that are easier to couple between but are known to have higher losses.[24,25]

Additionally, by decreasing the laser spot size and moving the substrate downward during deposition, it is possible to lift the deposition away from the substrate, resulting in a free-standing structure. This is due to glass' high molten viscosity allowing previously deposited fiber to be used as a support. As shown in Fig. 13 below, these free-standing structures retain some light-guiding capabilities, allowing for some unique photonic structures to be deposited in free space.

4 Conclusion

There has been significant work empirically defining how changes in the processing parameters of feed rate f, scan speed v, and laser power P affect the morphological parameters of SMF-28 deposited by DGF on a fused quartz substrate. To create strong bonds between the fiber feedstock and the substrate, high laser powers must be used, resulting in a significant change in the core and cladding geometry. By smoothly transitioning the deposition between the nominal and deformed fiber geometry, high transmission straight-line depositions were created. These slumped fiber geometries are also capable of guiding light around corners, but suffer from higher losses than lower processing power depositions at the same radius. There is evidence suggesting that depositing slumped fibers allows for the diffusion of the Ge-doped core into the cladding, leading to increased light leakage and higher losses. However, this can be compensated for using larger bending radii in component design. By altering the ratio of f to v, it is possible to achieve fine control of the resulting fiber area, which may allow for the depositions to be placed sufficiently close to each other for evanescent coupling between the fiber cores, creating additively manufactured photonic circuits.

Data Availability

Data underlying the results presented may be obtained from the authors upon reasonable request.

Acknowledgments

This work was supported by Los Alamos National Laboratory, Air Force Research Laboratory, and the National Science Foundation (Grant No. CMMI-1947391). This paper was presented at SPIE, Laser Applications in Microelectronic and Optoelectronic Manufacturing (LAMOM) XXVII, 119880E.

References

1. N. Kreidl, "Recent applications of glass science," *J. Non-Cryst. Solids* **123**, 377–384 (1990).
2. D. Hülsenberg, A. Harnisch, and A. Bismarck, "Silicate glasses: a class of amorphous materials," in *Microstructuring of Glasses*, Springer Series in Materials Science, R. Hull et al., Eds., Vol. **87**, Springer, Berlin, Heidelberg (2008).
3. Heraeus, "Data sheet: quartz glass for optics – data and properties," https://www.heraeus.com/media/media/hca/doc_hca/products_and_solutions_8/optics/Data_and_Properties_Optics_fused_silica_EN.pdf (2022).
4. G. Marchelli et al., "The guide to glass 3D printing: developments, methods, diagnostics, and results," *Rapid Prototyp. J.* **17**(3), 187–194 (2011).
5. F. Kotz et al., "Three-dimensional printing of transparent fused silica glass," *Nature* **544**, 337–339 (2017).
6. H.-R. Wang et al., "Alumina-doped silica gradient-index (GRIN) lenses by slurry-based three-dimensional printing (S-3DPTM)," *J. Non-Cryst. Solids* **349**, 360–367 (2004).
7. J. F. Destino et al., "3D printed optical quality silica and silica-titania glasses from sol-gel feedstocks," *Adv. Mater. Technol.* **3**, 1700323 (2018).
8. J. Klein et al., "Additive manufacturing of optically transparent glass," *3D Print. Addit. Manuf.* **2**(3), 92–105 (2015).
9. E. Gal-Or et al., "Chemical analysis using 3D printed glass microfluidics," *Anal. Methods* **11**, 1802–1810 (2019).
10. J. Luo, H. Pan, and E. C. Kinzel, "Additive manufacturing of glass," *J. Manuf. Sci. Eng.* **136**(6), 061024 (2014).
11. C. Liu, T. Oriekhov, and M. Fokine, "Investigation of glass bonding and multi-layer deposition during filament-based 3D printing," *Front. Mater.* **9**, 978861 (2022).
12. F. Kranert et al., "Generation of functional curved waveguides by CO_2-laser based deposition of coreless fused silica fibers," *Proc. SPIE* **11349**, 1134909 (2020).
13. W. Tian and W. Chiu, "Temperature prediction for CO_2 laser heating of moving glass rods," *Opt. Laser Technol.* **36**, 131–137 (2004).
14. Corning Inc., *Corning HPFS 7979, 7980, 8655 Fused Silica Optical Materials Product Information*, Corning, New York (2022).
15. J. Kaufman et al., "Structured spheres generated by an in-fibre fluid instability," *Nature* **487**, 463–467 (2012).
16. J. Noda, K. Okamoto, and Y. Sasaki, "Polarization-maintaining fibers and their applications," *J. Lightwave Technol.* **4**(8), 1071–1089 (1986).
17. L. Faustini and G. Martini, "Bend loss in single-mode fibers," *J. Lightwave Technol.* **15**, 671–679 (1997).
18. A. Harris and P. Castle, "Bend loss measurements on high numerical aperture single-mode fibers as a function of wavelength and bend radius," *J. Lightwave Technol.* **4**(1), 34–40 (1986).
19. D. Peters et al., "Sensing and control in glass additive manufacturing," *Mechatronics* **56**, 188–197 (2018).
20. S. Tsao and W. Cheng, "Simplified formula of bending loss for optical fiber sensors," *Fiber Integr. Opt.* **21**(5), 333–344 (2002).
21. C. Cardell and I. Guerra, "An overview of emerging hyphenated SEM-EDX and Raman spectroscopy systems: applications in life, environmental and materials sciences," *Trends Anal. Chem.* **77**, 156–166 (2016).
22. T. Kato, Y. Suetsugu, and M. Nishimura, "Estimation of nonlinear refractive index in various silica-based glasses for optical fibers," *Opt. Lett.* **20**(22), 2279–2281 (1995).
23. M. Digonnet and H. Shaw, "Analysis of a tunable single mode optical fiber coupler," *IEEE Trans. Microw. Theory Tech.* **30**(4), 592–600 (1982).
24. Corning Inc., *Corning Single-Mode Optical Fiber Product Information*, Corning, New York (2002).
25. J. Laferriere et al., *Reference Guide to Fiber Optic Testing*, Vol. **1**, JDS Uniphase Corporation, Milpitas, California (2007).

Nicholas Capps received his BS degree in AME from Missouri University of Science and Technology in 2018. He received his MS degree in 2022 and is currently pursuing his PhD in AME from the University of Notre Dame. His graduate work is focused on developing the digital glass forming technique for additive manufacturing of transparent silicate glasses.

Chen Zhu received his BS degree from Wuhan University, in 2013, and his master's degree from USTC, China, in 2017. Currently, he is pursuing his PhD in the Department of Aerospace and Mechanical Engineering, University of Notre Dame, Indiana, United States. His research interests include nanoscale fabrication and optics particularly toward controlling heat transfer.

Jonathan Goldstein received his PhD in physics from the University of Illinois at Urbana Champaign in 1996 and has been working since then at the Air Force Research Lab Materials and Manufacturing Directorate, in Dayton, Ohio, United States. During the last several years, he has focused on a variety of bulk glasses as well as laser treatments of glasses and ceramics, including laser sintering of ceramic YAG fiber, selective laser sintering of silica powders, and glass fiber processing for fiber-fed laser-fused deposition.

Edward Kinzel received his PhD in mechanical engineering from Purdue University in 2010. He was on the faculty at Missouri S&T from 2012 to 2018 before coming to the University of Notre Dame in 2019 as an associate professor. His current research focuses on laser processing, including additive manufacturing of glass and optical diagnostics for laser powder bed fusion. He also works on combined thermal/electromagnetic design of IR antennas and the scalable manufacturing of metasurfaces.